

## LETTER

# Zeeman- and electric-field control of spin- and valley-polarized transport through biased magnetic junctions on WSe<sub>2</sub>

To cite this article: M. Tahir *et al* 2017 *EPL* **118** 17001

View the [article online](#) for updates and enhancements.

## Related content

- [Optical, electric and magnetic controlled ballistic conductance in monolayer WSe<sub>2</sub>: the perfect valley and spin polarizations](#)  
X J Qiu, Q Lv and Z Z Cao

- [Spin and valley-dependent electron transport through arrays of ferromagnet on monolayer MoS<sub>2</sub>](#)  
X J Qiu, Z Z Cao, Y F Cheng et al.

- [A valley and spin filter based on gapped graphene](#)  
Jing Wang, Mengqiu Long, Wen-Sheng Zhao et al.

# Zeeman- and electric-field control of spin- and valley-polarized transport through biased magnetic junctions on WSe<sub>2</sub>

M. TAHIR<sup>1(a)</sup>, P. M. KRSTAJIĆ<sup>2(b)</sup> and P. VASILOPOULOS<sup>3(c)</sup>

<sup>1</sup> Department of Physics, College of Science, University of Hafr Al Batin - P.O. Box 1803, Hafr Al Batin 31991, Kingdom of Saudi Arabia

<sup>2</sup> Center of Microelectronic Technologies and Single Crystals (IHTM), University of Belgrade Njegoševa 12, 11000 Belgrade, Serbia

<sup>3</sup> Department of Physics, Concordia University - 7141 Sherbrooke West, Montreal, Quebec, H4B 1R6, Canada

received 27 February 2017; accepted in final form 10 May 2017  
published online 30 May 2017

PACS 73.40.Gk – Tunneling

PACS 74.55.+v – Tunneling phenomena: single particle tunneling and STM

PACS 72.25.-b – Spin polarized transport

**Abstract** – The electronic properties of WSe<sub>2</sub> comprise a huge spin-orbit coupling, a wide direct band gap, and especially a strong anisotropic lifting of the degeneracy of the valley degree of freedom in a magnetic field. We study ballistic electron transport through single or double junctions on monolayer WSe<sub>2</sub> in the presence of spin  $M_s$  and valley  $M_v$  Zeeman fields and of an electric potential  $U$ . The conductance *vs.* the field  $M_s$  or  $M_v$  decreases in a fluctuating manner. For a single junction the spin  $P_s$  and valley  $P_v$  polarizations rise with  $M = M_v = 2M_s$ , reach a value of more than 70%, and *become perfect* above  $U \approx 90$  meV while for a double junction this change can occur for  $U \approx 50$  meV and  $M \geq 10$  meV.  $P_v$  increases with  $U$  and both polarizations oscillate with the junction width. The results may render WSe<sub>2</sub> a promising candidate for new spintronic and valleytronic devices.

Copyright © EPLA, 2017

**Introduction.** – Currently there is a strong interest in two-dimensional (2D) systems as potential hosting materials for applications in spintronics and valleytronics [1]. Similar to graphene [2], the first hexagonal Brillouin zone of group-VI monolayer transition metal dichalcogenides (TMDs) (*e.g.*, MX<sub>2</sub>, M = Mo, W; X = S, Se, Te) [3–7] accommodates pairs of inequivalent valleys. Distinctively, the monolayer MX<sub>2</sub> exhibits a huge gap and strong spin-orbit coupling (SOC). This enables valley-dependent optical selection rules which allow for valley polarization and spin-valley coupling. The valence and conduction band extrema are located at both  $K$  and  $K'$  valleys at the corners of the hexagonal Brillouin zone and give rise to the valley degree of freedom of the band-edge electrons and holes [8–11]. In contrast to the extensive theoretical [12] and experimental efforts on spin- and valley-controlled applications of MoS<sub>2</sub> as well as silicene [13–15], the high quality of WSe<sub>2</sub> [16] and its much stronger SOC,

$2\lambda'_v = 450$  meV in the valence band and  $2\lambda'_c = 30$  meV in the conduction band, provide an excellent system for spin-valley controlled materials [17,18]. Although monolayer WSe<sub>2</sub> is a direct bandgap semiconductor ( $2\Delta = 1.7$  eV), the lifting of the valley degeneracy allows for optical manipulation of the electron valley index or degree of freedom, *e.g.*, by an external magnetic field applied perpendicular to the 2D layer [17,18]. The lifting of the valley degeneracy in WSe<sub>2</sub> monolayers is achieved by monitoring the energy splitting between the two circularly polarized luminescence components,  $\sigma^+$  and  $\sigma^-$ , associated with optical recombination in the non-equivalent valleys. Direct optical transitions in monolayer WSe<sub>2</sub> occur at the edge of the Brillouin zone, which mainly consists of strongly localized  $d$ -orbitals of the transition metal. This is in contrast with GaAs and other conventional semiconductors used in optoelectronics, where the direct optical band gap is situated at the centre of the Brillouin zone. In monolayer WSe<sub>2</sub> there are several possible contributions to the Zeeman splitting as the emission of circularly polarized light originates from states with contrasting valley index, spin, and orbital magnetic moment. Moreover, recently

(a) E-mail: m.tahir06@alumni.imperial.ac.uk

(b) E-mail: predrag222@gmail.com

(c) E-mail: p.vasilopoulos@concordia.ca

WSe<sub>2</sub> transistors have been demonstrated to have high mobility at room temperature [19]. In addition, the advantage of WSe<sub>2</sub> over, for example, silicene, is that we do not need large perpendicular electric fields [15] to achieve a significant gap. Valley-polarized transport in WSe<sub>2</sub> has been investigated in ref. [20], while spin-valley relaxation and quantum transport regimes in 2D transition-metal dichalcogenides has been treated in ref. [21]. It is also worth mentioning the study of local Andreev reflection in a MoS<sub>2</sub>-based bipolar transistor [22], where pure valley- and spin-entangled states have been predicted.

We theoretically study valley- and spin-polarized transport through a single or double magnetic junction or barrier in monolayer WSe<sub>2</sub>. We find that *fully* valley- and spin-polarized currents can be obtained simultaneously through such junctions for certain ranges of the relevant Zeeman and electric fields. We emphasize that the spin splitting near the valence-band edges is essential to the valley-polarized transport. At zero voltage we show that it is possible to achieve spin  $P_s$  and  $P_v$  valley polarizations close to 30% for reasonable values of  $M_s$  and  $M_v$ . Applying a voltage to the barrier one can achieve  $P_v \approx 85\%$  and  $P_s \approx 70\%$ . Perfect polarizations can be reached for  $M \geq 10$  meV and  $U \geq 80$  meV. For double barriers the behaviour of the conductance is similar to that of a single barrier but  $P_v$  and  $P_s$  can become perfect for  $M \geq 10$  meV and  $U \geq 50$  meV. The details are as follows.

**Transmission, conductance, and polarizations.** – We consider a monolayer of WSe<sub>2</sub> in the  $(x, y)$ -plane in the presence of intrinsic SOC, spin and valley Zeeman fields. The 2D Dirac-like Hamiltonian [16] of WSe<sub>2</sub> is

$$H_{s_z}^\eta = v(\eta\sigma_x p_x + \sigma_y p_y) + \Delta\sigma_z + \eta s_z(\lambda_c\sigma_+ + \lambda_v\sigma_-) + s_z M_s - \eta M_v + U(x). \quad (1)$$

Here  $\eta = \pm 1$  for valleys  $K$  and  $K'$ ,  $\Delta$  is the mass term that breaks the inversion symmetry,  $\lambda_c = \lambda'_c/2$ ,  $\lambda_v = \lambda'_v/2$ . Furthermore,  $(\sigma_x, \sigma_y, \sigma_z)$  are the Pauli matrices for the valence and conduction bands, and  $\sigma_\pm = \sigma_0 \pm \sigma_z$  ( $\sigma_0$  is the unity matrix);  $v$  ( $5 \times 10^5$  m/s) denotes the Fermi velocity of Dirac fermions. Spins up and down are denoted by  $s_z = +1$  and  $-1$ , respectively. Further,  $M_s$  is the Zeeman field induced by magnetic order, while  $M_v$  breaks the valley symmetry of the levels. In principle, they can be induced by an external magnetic field,  $M_s = g'\mu_B B/2$ ,  $M_v = g_v\mu_B B/2$ , where  $g'$  is the Landé  $g$ -factor ( $g' = g'_e + g'_s$ ), and  $\mu_B$  the Bohr magneton [17,18]. Also,  $g'_e = 2$  is the free-electron  $g$ -factor and  $g'_s = 0.21$  is the out-of-plane factor due to the strong SOC in WSe<sub>2</sub>. The last term in eq. (1) is the electric potential applied to the magnetic barrier. For a single barrier we have  $U(x) = U$  in region II and  $U(x) = 0$  elsewhere. Finally, for the valley degree freedom one has  $g'_v = 4$  [17,18]. In addition, an enhanced valley splitting can be achieved by an interfacial magnetic field produced by placing a monolayer WSe<sub>2</sub> on a substrate made of magnetic EuS [23]. We note at this point that relatively long carrier diffusion

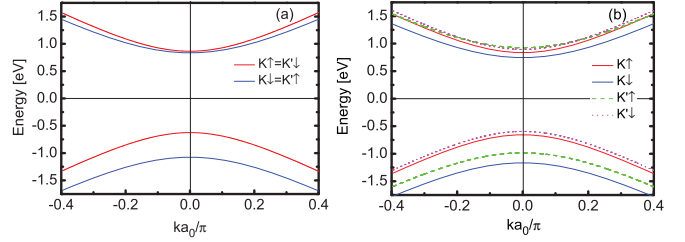


Fig. 1: (Colour online) Dispersion  $E(k)$  in WSe<sub>2</sub>, for (a)  $M_s = M_v = 0$ , and (b)  $M_s = 30$  meV and  $M_v = 60$  meV. In both panels  $\Delta = 0.85$  eV,  $\lambda_v = 112.5$  meV, and  $\lambda_c = 7.5$  meV.

lengths (380 nm) have been reported [24] for monolayer WSe<sub>2</sub>, which enables us to treat ballistic transport.

The eigenvalues of the Hamiltonian (1) are given by

$$E_{s_z,t}^\eta = \eta s_z(\lambda_c + \lambda_v) + s_z M_s - \eta M_v + U(x) + t E_{s_z}^\eta, \quad (2)$$

with  $E_{s_z}^\eta = [(\hbar v k)^2 + [\Delta + \eta s_z(\lambda_c - \lambda_v)]^2]^{1/2}$ . The corresponding eigenfunctions are

$$\Psi_{s_z,t}^\eta = (e^{i\mathbf{k}\cdot\mathbf{r}}/D_k) \begin{pmatrix} \eta c_k e^{-\eta i\theta} \\ b_k \end{pmatrix}, \quad (3)$$

where  $c_k = \hbar v k$ ,  $b_k = -\Delta - \eta s_z(\lambda_c - \lambda_v) + t E_{s_z}^\eta$ ,  $D_k = [c_k^2 + [\Delta + \eta s_z(\lambda_c - \lambda_v) - t E_{s_z}^\eta]^2]^{1/2}$ , and  $\theta = \tan^{-1}(k_y/k_x)$ . Further,  $t = 1(-1)$  denotes the conduction (valence) band, and  $k$  is the 2D wave vector. Notice that there is no external magnetic field in eq. (2) but we have considered the spin and valley Zeeman field as discussed in detail below eq. (1).

The spectrum (2) is shown in fig. 1 *vs.*  $ka_0$  (where  $a_0 = 0.331$  nm is the lattice constant) for two cases: (a)  $M_s = M_v = 0$  and (b)  $M_s = 30$  meV and  $M_v = 60$  meV. As can be seen, the valence band has a larger splitting even when the Zeeman field is present. We find that there is a valley asymmetry due to the application of magnetic field. This can be understood from the valley Zeeman term  $M_v$  in eq. (2) which makes the two valleys non-degenerate in both bands. This clearly confirms the magnetic-field-controlled valley pseudospin degree of freedom in WSe<sub>2</sub>.

We now use these considerations to study ballistic electron transport across a magnetic junction in WSe<sub>2</sub> with a metallic gate only above it, see fig. 2. We assume that regions I and III in fig. 2 are made of the usual WSe<sub>2</sub> (no Zeeman field,  $M_s = M_v = 0$  and no potential barrier  $U(x) = 0$ ), while a magnetic barrier is placed in region II ( $U(x) \neq 0$ ) in which the full Hamiltonian (1) applies. For  $x < 0$  the wave functions are

$$\Psi_1(x, y) = e^{i\mathbf{k}\cdot\mathbf{r}} \begin{pmatrix} A_1 e^{-i\eta\theta} \\ B_1 \end{pmatrix} + r_{\eta s_z} e^{i(-k_x x + k_y y)} \begin{pmatrix} A_1 e^{-i\eta(\pi-\theta)} \\ B_1 \end{pmatrix}, \quad (4)$$

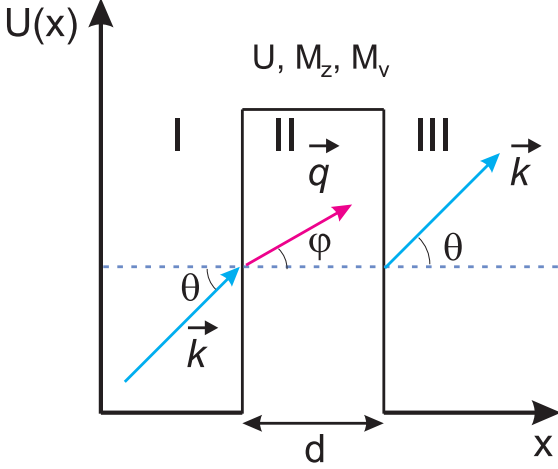


Fig. 2: (Colour online) Schematics of a single barrier, of width  $d$ , on WSe<sub>2</sub>.  $M_s$ ,  $M_v$ , and  $U(x)$  are finite in region II and vanish elsewhere.

where  $A_1 = \eta c_k/D_k$  and  $B_1 = b_k/D_k$ . The result

$$\Psi_2(x, y) = P e^{i(q_x x + k_y y)} \begin{pmatrix} A_2 e^{-i\eta\varphi} \\ B_2 \end{pmatrix} + Q e^{i(-q_x x + k_y y)} \begin{pmatrix} A_2 e^{-i\eta(\pi - \varphi)} \\ B_2 \end{pmatrix}. \quad (5)$$

is for  $0 < x < d$ . Finally, for  $x > d$ , we have

$$\Psi_3(x, y) = t_{\eta s_z} e^{i\mathbf{k} \cdot \mathbf{r}} \begin{pmatrix} A_1 e^{-i\eta\theta} \\ B_1 \end{pmatrix}. \quad (6)$$

Here  $A_2 = \eta c_q/D_q$ ,  $c_q = \hbar v(q_x^2 + k_y^2)^{1/2}$ , and  $D_q = [c_q^2 + [-\Delta - \eta s_z(\lambda_c - \lambda_v) + tE_{s_z}^\eta(q_x, k_y)]^2]^{1/2}$ . Also,  $B_2 = b_q/D_q$  and  $b_q = -\Delta - \eta s_z(\lambda_c - \lambda_v) + tE_{s_z}^\eta(q_x, k_y)$ . Further,  $\theta$  and  $\varphi$  are the angles of incidence and reflection given by  $\theta = \tan^{-1}(k_y/k_x)$ ,  $k_x = k_F \cos \theta$ ,  $k_y = k_F \sin \theta$ , with  $k_F$  the Fermi momentum,  $q_x = [k_F^2 - k_y^2]^{1/2}$ , and  $\varphi = \tan^{-1}(k_y/q_x)$ .  $k'_F$  includes the changes in potential or/and Zeeman field, while the wave vector  $k_y$  and the energy  $E$  are conserved.

The coefficients  $r_{\eta s_z}$ ,  $P$ ,  $Q$  and  $t_{\eta s_z}$  are determined by the continuity of the wave functions at the interfaces, *i.e.*,

$$\Psi_I(0-, y) = \Psi_{II}(0+, y), \quad \Psi_{II}(d-, y) = \Psi_{III}(d+, y). \quad (7)$$

The resulting transmission  $T_{\eta s_z} = |t_{\eta s_z}|^2$  reads

$$T_{\eta s_z} = 1 / [1 + \sin^2(q_x d)(F^2(\gamma, \theta, \varphi) - 1)], \quad (8)$$

where  $\gamma = k_F b_q/(k'_F b_k)$  and  $F(\gamma, \theta, \varphi) = (\gamma + \gamma^{-1} - 2 \sin \theta \sin \varphi)/(2 \cos \theta \cos \varphi)$ .

Now we are ready to evaluate the conductance due to a particular spin and valley; it is given by

$$G_{\eta s_z} = G_0 \int_{-\pi/2}^{\pi/2} T_{\eta s_z}(\theta) \cos \theta d\theta = G_0 g_{c\eta s_z}, \quad (9)$$

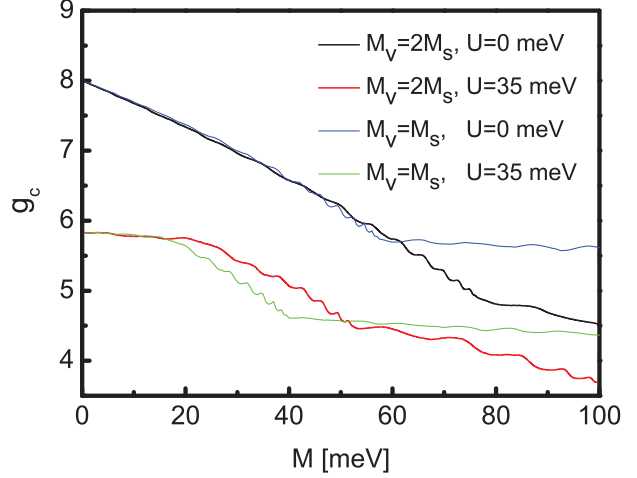


Fig. 3: (Colour online) Conductance *vs.*  $M = M_v = 2M_s$  (black and red curves) and *vs.*  $M = M_v = M_s$  (blue and green curves) with  $E_F = 0.95$  eV and  $U = 0$  meV or  $U = 35$  meV as indicated.

where  $G_0 = e^2 k_F W / (2\pi\hbar)$ , and  $W$  is the width along the  $y$ -direction. Furthermore, the spin  $P_s$  and valley  $P_v$  polarizations are defined as

$$P_s = \frac{g_{c\uparrow} - g_{c\downarrow}}{g_{c\uparrow} + g_{c\downarrow}} \quad \text{and} \quad P_v = \frac{g_{cK} - g_{cK'}}{g_{cK} + g_{cK'}}. \quad (10)$$

Below we will present various results for the conductance and polarizations. In the calculations we use the Fermi energy  $E_F$  for which both spin states and valleys in regions I and III are occupied.

**Results and discussion.** – In fig. 3 we show the total conductance  $g_c$  *vs.* the Zeeman field  $M$  given in the caption. The various curves are marked in the inset by the values of  $M_s$ ,  $M_v$ , and  $U$  used. The Fermi level is  $E_F = 0.95$  eV. For  $U = 0$  the conductance  $g_c$  decreases with  $M$  but the decrease weakens considerably for  $U \neq 0$  and  $M \geq 20$  meV (lower curves) or  $M \geq 60$  meV (upper curves).

Next we present results in fig. 4 for the spin  $P_s$  (red solid curve) and valley  $P_v$  (blue dashed curve) polarizations *vs.* barrier width  $d$ . The left panels are for  $M_s = 30$  meV and  $M_v = 60$  meV, while the right panels are for  $M_s = 60$  meV and  $M_v = 30$  meV. Also two values of the potential are considered,  $U = 0$  meV (upper panels) and  $U = 45$  meV (lower panels). As expected, both polarizations start from zero for vanishing  $d$ . As  $d$  increases they rise and attain some values around which they oscillate. If we use  $M_s = M_v = 60$  meV, we obtain  $P_v = |P_s| \approx 30\%$ , for  $U = 0$  meV, and  $P_v = |P_s| \approx 40\%$  for  $U = 45$  meV. In all cases the oscillations result from two oscillating terms that depend on different propagating wave vectors for two different spin/valley indices in region II. We note that  $|P_s| > |P_v|$  whenever  $M_s > M_v$  and vice versa. Moreover, it can be seen that an applied voltage raises  $P_v$  above 80%

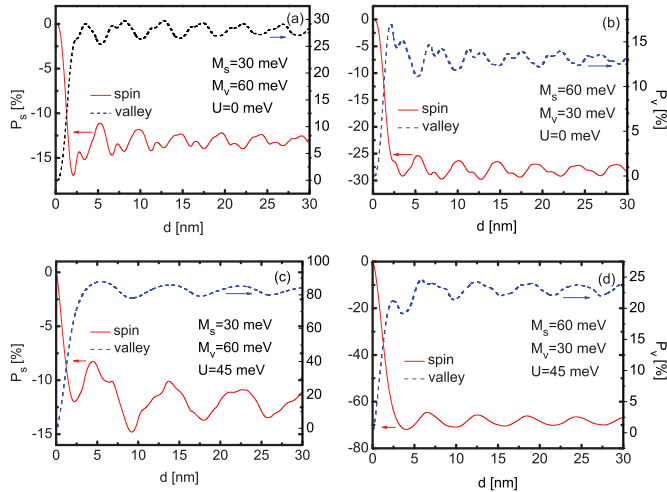


Fig. 4: (Colour online) Spin (red curve) and valley (blue) polarization as functions of the barrier width  $d$ , for  $M_s = 30$  meV,  $M_v = 60$  meV (left panels), and  $M_s = 60$  meV,  $M_v = 30$  meV (right panels). The upper panels are for  $U = 0$ , the lower ones for  $U = 45$  meV, and all for  $E_F = 0.95$  eV.

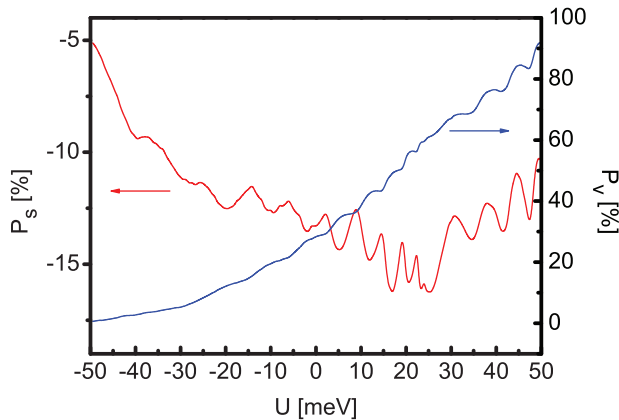


Fig. 5: (Colour online) Polarizations  $P_s$  and  $P_v$  vs. potential  $U$  for  $E_F = 0.95$  eV,  $d = 30$  nm, and  $M_v = 2M_s = 60$  meV.

and  $|P_s|$  close to 70%. As for the opposite signs of  $P_s$  and  $P_v$ , they are due to the term  $s_z M_s - \eta M_v$  in eq. (1).

Further, we investigate the influence of applying a voltage  $U$  in region II while keeping other parameters fixed. In fig. 5 we show  $P_s$  and  $P_v$  as functions of the applied voltage  $U$  for  $E_F = 0.95$  eV,  $d = 30$  nm,  $M_s = 30$  meV and  $M_v = 60$  meV. The valley polarization rises with increasing voltage  $U$  and attains a value close to 90%, for  $U = 50$  meV, while  $|P_s|$  increases up to 18% for  $U \approx 25$  meV but then decreases. The lower maximal values of  $|P_s|$  compared to those of  $|P_v|$  occur because we assumed  $M_v > M_s$ ; if we use  $M_v < M_s$  we obtain the opposite behaviour, *i.e.*,  $|P_v| < |P_s|$ .

In order to investigate the combined influence of the Zeeman fields and applied voltage on both polarizations, we show contour plots of  $P_s$  in fig. 6(a) and of  $P_v$  in fig. 6(b) (we set  $M_s = M_v$ ). We see that  $P_v$  becomes

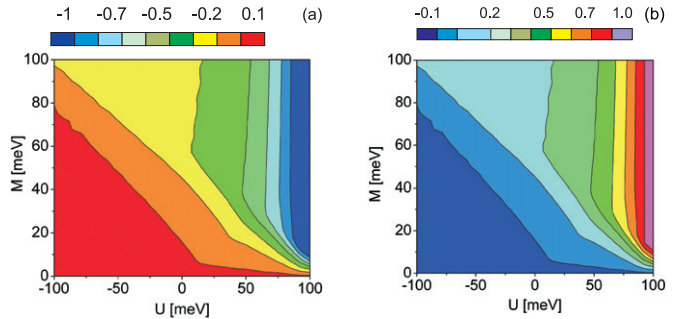


Fig. 6: (Colour online) ( $M, U$ ) contour plots of (a) spin polarization; (b) valley polarization. Both panels are for  $E_F = 0.95$  eV and barrier width  $d = 30$  nm ( $M_s = M_v$ ).

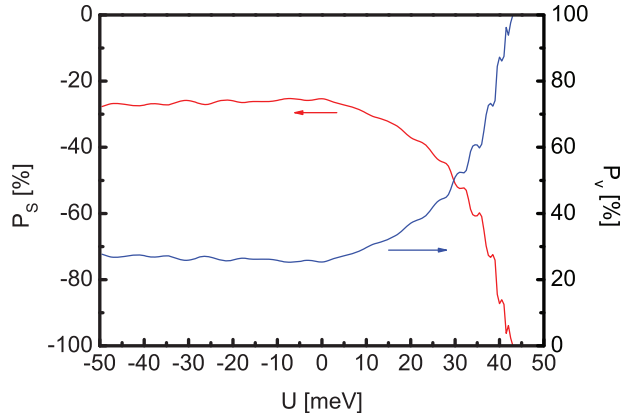


Fig. 7: (Colour online) Spin (red curve) and valley (blue curve) polarization vs. gate voltage  $U$  for a double-barrier structure and barrier separation  $b = 30$  nm. The Fermi level is  $E_F = 0.95$  eV and the barrier width  $d = 30$  nm ( $M_s = M_v$ ).

perfect for  $M \geq 15$  meV and large  $U \geq 90$  meV (magenta region), and  $|P_s|$  for  $M \geq 10$  meV and  $U \geq 85$  meV (dark-blue region). Notice that the colour codes are different in the two panels and that in other regions  $P_v$  and  $|P_s|$  attain high values, in the range from 70% to 90%, for lower values of  $U$  though mostly for higher values of  $M$ .

We proceed by considering two junctions or barriers separated by a normal WSe<sub>2</sub> layer, of thickness  $b$  and different values of the Zeeman fields and bias,  $M, U$  in the first,  $2M, 2U$  in the second, with  $M_s = M_v = M$ . In fig. 7 we show the results for such a structure: the red curve shows the spin polarization and the blue one the valley polarization as functions of the applied voltage  $U$ . The barrier width ( $d$ ) and separation ( $b$ ) are  $d = b = 30$  nm, and  $M = 60$  meV, while the Fermi level is  $E_F = 0.95$  eV. As shown, high polarizations (in absolute sense) can be achieved for  $U > 40$  meV.

Next, in fig. 8 we plot  $P_s$  (red curve) and  $P_v$  (blue curve) vs. the Zeeman field  $M_v = 2M_s = M$ . The left panel is for  $U = 0$  meV and the right one for  $U = 35$  meV. Both polarizations exhibit less monotonic behaviour. These results show that with an appropriate applied voltage one

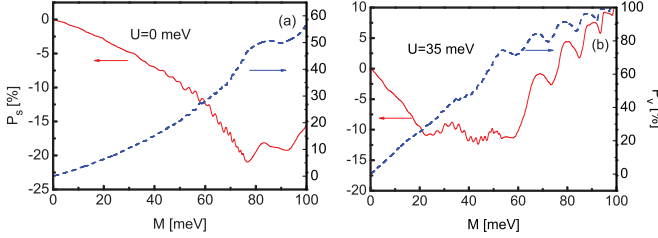


Fig. 8: (Colour online) Polarizations, as indicated, as functions of the Zeeman field  $M_v = 2M_s = M$ , for  $E_F = 0.95$  eV, and  $b = 30$  nm. The left panel is for  $U = 0$  and the right one for  $U = 35$  meV.

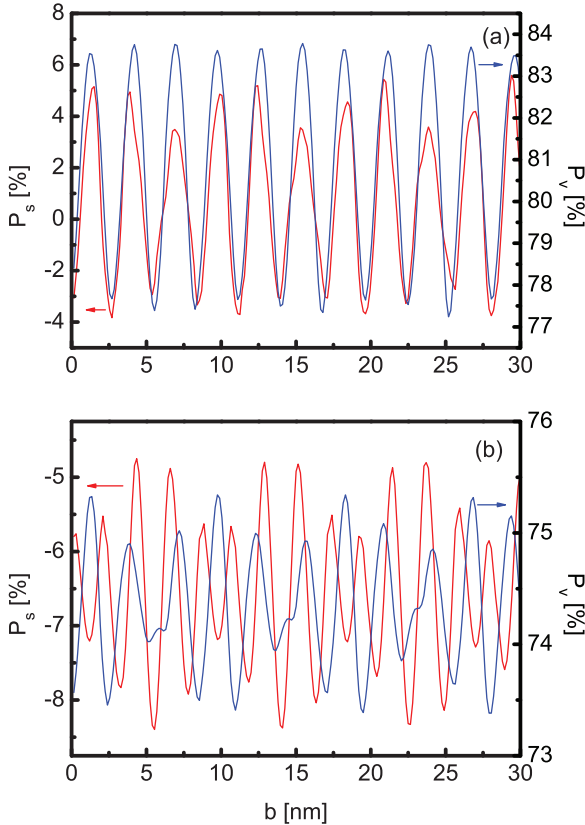


Fig. 9: (Colour online) Polarizations, as indicated, as functions of the normal layer width  $b$  for  $M_v = 2M_s = M$ ,  $E_F = 0.95$  eV, and  $d = 30$  nm. The upper panel is for  $(M, U) = (30, 20)$  meV and the lower one for  $(M, U) = (60, 5)$  meV.

can increase the valley polarization close to 100% for  $M = 100$  meV.

We also varied the width  $b$  in the range (0–30) nm and show both polarizations in fig. 9, for two sets of  $(M, U)$  values: (a)  $(100, -12)$  meV and (b)  $(60, 5)$  meV. One can see that  $P_v$  shows regular oscillations in panel (a) but less regular in panel (b). In both cases the relative change is not large, about 6%. As for  $P_s$ , its oscillations in panel (b) are about a factor of 2 smaller than in panel (a). Finally, in fig. 10 we show  $(M, U)$  contour plots of  $P_s$  and  $P_v$ , for two barriers ( $M_s = M_v = M$ ), as in fig. 7, when both  $M$  and  $U$  are varied. Comparing with the single-barrier case one

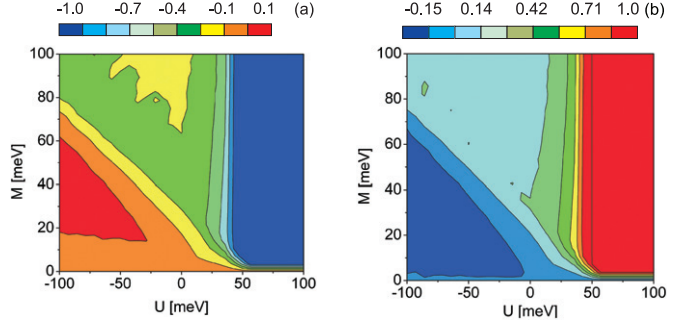


Fig. 10: (Colour online)  $(M, U)$  contour plots of the double-barrier case: (a) spin polarization; (b) valley polarization. Both panels are for  $E_F = 0.95$  eV, barrier width  $d = 30$  nm, and barrier separation  $b = 30$  nm.

can conclude that high values of  $P_s$  and  $P_v$  (in absolute sense) are obtainable in wider regions of the  $(M, U)$ -plane. One can see that perfect  $P_v$  and  $|P_s|$  are achievable for  $M \geq 5$  meV and  $U$  close to 50 meV or higher, see blue region in the left panel and the red one in the left panel.

In summary, we studied the Zeeman- and electric-field-controlled spin- and valley-polarized transport through biased, single or double magnetic junctions on monolayer WSe<sub>2</sub>. The degree of polarization depends on the values of  $M_s$ ,  $M_v$ , and  $U$ . We showed that *fully* valley- and spin-polarized currents can be obtained simultaneously in such junctions in some ranges of the parameters involved, especially for double junctions, cf. fig. 8. Physically in WSe<sub>2</sub> junctions, the Zeeman field opens different spin-dependent band gaps at the  $K$  and  $K'$  valleys, which, in turn, induce spin- and valley-polarized currents. By interchanging the values of  $M_s$  and  $M_v$  the values of  $P_s$  and  $P_v$  are interchanged but, though not shown, the total conductance remains the same. As functions of the junction width the polarizations rise and attain certain values, which can be in the range from 70% to 85% when a voltage is applied, around which they oscillate. Their values also depend on the Fermi energy  $E_F$  used; though not shown, in general they decrease with  $E_F$ . All these results confirm the magnetic and electric control of the polarizations and contribute significantly to the fundamental investigations of the electronic properties of 2D WSe<sub>2</sub>. As such, they may be very relevant to the design of spintronic and valleytronic devices.

\*\*\*

This work was supported by the University of Hafr Al Batin (MT), the Ministry of Education, Science, and Technological development of Serbia within the Project No. TR 32008 (PMK), and the Canadian NSERC Grant No. OGP0121756 (PV).

## REFERENCES

- [1] XU X., YAO W., XIAO D. and HEINZ T. F., *Nat. Phys.*, **10** (2014) 343.

- [2] LIAO L., LIN Y.-C., BAO M., CHENG R., BAI J., LIU Y., QU Y., WANG K. L., HUANG Y. and DUAN X., *Nature*, **467** (2010) 305; SCHWIERZ F., *Nat. Nanotechnol.*, **5** (2010) 487.
- [3] GEIM A. K. and GRIGORIEVA I. V., *Nature*, **499** (2013) 419.
- [4] FANG H., CHUANG S., CHANG T. C., TAKEI K., TAKAHASHI T. and JAVEY A., *Nano Lett.*, **12** (2012) 3788; WANG H., YU L., LEE Y.-H., SHI Y., HSU A., CHIN M. L., LI L.-J., DUBEY M., KONG J. and PALACIOS T., *Nano Lett.*, **12** (2012) 4674; FUHRER M. S. and HONE J., *Nat. Nanotechnol.*, **8** (2013) 146.
- [5] LU H.-Z., YAO W., XIAO D. and SHEN S.-Q., *Phys. Rev. Lett.*, **110** (2013) 016806.
- [6] LI X., ZHANG F. and NIU Q., *Phys. Rev. Lett.*, **110** (2013) 066803.
- [7] ZHANG Q., YANG S. A., MI W., CHENG Y. and SCHWINGENSCHLÖGL U., *Adv. Mater.*, **28** (2016) 959.
- [8] SPLENDIANI A., SUN L., ZHANG Y., LI T., KIM J., CHIM C.-Y., GALLI G. and WANG F., *Nano Lett.*, **10** (2010) 1271.
- [9] ELLIS J. K., LUCERO M. J. and SCUSERIA G. E., *Appl. Phys. Lett.*, **99** (2011) 261908.
- [10] LEE H. S., MIN S.-W., CHANG Y.-G., PARK M. K., NAM T., KIM H., KIM J. H., RYU S. and IM S., *Nano Lett.*, **12** (2012) 3695.
- [11] CAPPELLUTI E., ROLDÁN R., SILVA-GUILLÉN J. A., ORDEJÓN P. and GUINEA F., *Phys. Rev. B*, **88** (2013) 075409.
- [12] Li H., SHAO J., YAO D. and YANG G., *ACS Appl. Mater. Interfaces*, **6** (2014) 1759.
- [13] YOKOYOMA T., *Phys. Rev. B*, **87** (2013) 241409(R).
- [14] VARGIAMIDIS C. and VASILOPOULOS P., *J. Appl. Phys.*, **117** (2015) 094305; *Appl. Phys. Lett.*, **105** (2014) 223105.
- [15] MISSAULT N., VASILOPOULOS P., VARGIAMIDIS C., PEETERS F. M. and VAN DUPPEN B., *Phys. Rev. B*, **92** (2015) 195423.
- [16] JONES A. M., YU H., ROSS J. S., KLEMENT P., GHIMIRE N. J., YAN J., MANDRUS D. G., YAO W. and XU X., *Nat. Phys.*, **10** (2014) 130.
- [17] AIVAZIAN G., GONG Z., JONES A. M., CHU R.-L., YAN J., MANDRUS D. G., ZHANG C., COBDEN D., YAO W. and XU X., *Nat. Phys.*, **11** (2015) 148.
- [18] SRIVASTAVA A., SIDLER M., ALLAIN A. V., LEMBKE D. S., KIS A. and IMAMOĞLU A., *Nat. Phys.*, **11** (2015) 141.
- [19] MOVVA H. C. P., RAI A., KANG S., KIM K., FALLAHAZAD B., TANIGUCHI T., WATANABE K., TUTUC E. and BANERJEE S. K., *ACS Nano*, **9** (2015) 10402.
- [20] ZHANG L., GONG K., CHEN J., LIU L., ZHU Y., XIAO D. and GUO H., *Phys. Rev. B*, **90** (2014) 195428.
- [21] OCHOA H., FINOCCHIARO F., GUINEA F. and FALKO V. I., *Phys. Rev. B*, **90** (2014) 235429.
- [22] BAI C., ZOU Y., LOU W.-K. and CHANG K., *Phys. Rev. B*, **90** (2014) 195445.
- [23] ZHAO C., NORDEN T., ZHAO P., CHENG Y., ZHANG P., SUN F., TAHERI P., WANG J., YANG Y., SCRACE T., KANG K., YANG S., MIAO G.-X., SABIRIANOV R., KIOSEOGLOU G., PETROU A. and ZENG H., arXiv:cond-mat/1610.04878 (2016).
- [24] CUI Q., CEBALLOS F., KUMAR N. and ZHAO H., *ACS Nano*, **8** (2014) 2970.